PHYSICAL REVIEW A VOLUME 38, NUMBER 5 SEPTEMBER 1, 1988

Nonlinear transport processes and fluid dynamics: Cylindrical Couette flow of Lennard-Jones fluids

R. E. Khayat and Byung Chan Eu*
Department of Chemistry, McGill University, 801 Sherbrooke Street West, Montreal, Quebec, Canada H3A 2K6
(Received 8 February 1988)

In this paper we report on calculations of flow profiles for cylindrical Couette flow of a Lennard-Jones fluid. The flow is subjected to a temperature gradient and thermoviscous effects are taken into consideration. We apply the generalized fluid dynamic equations which are provided by the modified moment method for the Boltzmann equation reported previously. The results of calculations are in good agreement with the Monte Carlo direct simulation method by K. Nanbu [Phys. Fluids **27**, 2632 (1984)] for most of Knudsen numbers for which the simulation data are available.

I. INTRODUCTION

We have studied in a previous paper[1] the effects of nonlinear viscosity and heat conduction on velocity and temperature profiles in plane Couette flow of a Lennard-Jones fluid. Since flow profiles are not measured in practice in plane Couette flow geometry, the lack of experimental data prevented us from making experimental comparison of the theoretically computed profiles. In this work we report on calculations of flow profiles for cylindrical Couette flow of a Lennard-Jones fluid and comparison of the results with experiment. As in the previous works[1,2] we apply the generalized fluid dynamic equations which are provided by the modified moment method[3] for the Boltzmann equation and the generalized Boltzmann equation reported previously. The profiles calculated with the generalized hydrodynamic equations are compared with experimental ones,[4] those by Navier-Stokes theory with slip boundary conditions, and those by Nanbu[5] who used a direct simulation method for the Boltzmann equation. The comparison with numerical results and the Navier-Stokes results with slip boundary conditions are generally good for most of Knudsen numbers considered by Nanbu, but in the case of experimental comparison there occur, as in the case of Nanbu's simulation results, significant deviations as the Knudsen number gets large. The present numerical results therefore indicate that the particular forms of generalized hydrodynamic equations used here are applicable in the domain of relatively low Knudsen numbers as is the direct simulation method used by Nanbu. The fact that the results are comparable with those by the direct simulation method and the Navier-Stokes theory with slip boundary conditions renders support for the use of the stick boundary conditions together with the nonlinear constitutive equations for stress tensors and heat fluxes which the particular generalized hydrodynamic equations taken for this work imply.

The generalized hydrodynamic equations used are provided by the modified moment method[3] and conform to the thermodynamic laws since they are within the framework of extended irreversible thermodynamics. As will be shown, they reduce to the classical Navier-Stokes and Fourier equations as the product of the Mach and Knudsen numbers tends to zero. Since the Knudsen number is inversely proportional to the density of the fluid, as the fluid density decreases, the Knudsen number increases and the generalized hydrodynamic equations increasingly deviate from those of classical forms. Such deviations are generally represented by terms which are nonlinear in stress tensors, heat fluxes, or thermodynamic gradients. The presence of such terms makes the generalized hydrodynamic equations highly nonlinear.

In the conventional theory[6] of rarefied gas dynamics the deviations of flow profiles from those predicted by the Navier-Stokes and Fourier equations are accounted for by modifying the boundary conditions from stick to slip boundary conditions or by solving the kinetic equation in terms of half-range velocity distribution functions with diffuse and specular boundary conditions which lead to slip boundary conditions. In the present approach a similar effect is achieved, as will be shown, with combination of stick boundary conditions and nonlinear transport coefficients or nonlinear constitutive equations for stress tensors and heat fluxes associated with various flow processes. This represents a significant departure from the conventional approach, but the calculated profiles agree with those by Nanbu's direct simulation method[5] and the Navier-Stokes theory with slip boundary conditions, confirming the validity of the method and the boundary conditions taken. This validity test was not possible to make in the previous works[1,2] for the lack of available data as mentioned earlier.

In Sec. II we present the basic equations provided by the modified moment method. Then these equations are cast in reduced form in which the product of Mach and Knudsen number appears as an order parameter. On the basis of the order parameter, we obtain an approximate set of generalized hydrodynamic equations which are then solved by a numerical method in cylindrical Couette flow geometry. Since the boundary conditions occupy an important place in gas dynamics, they are discussed in some detail in Sec. II. Comparison with the results by a direct simulation method, the Navier-Stokes theory and experiment is made in Sec. III where we will also discuss some aspects of the direct simulation method in an effort to understand the relative merits of the present method. This discussion will also shed light on the range of appli-

cability of the direct simulation method used by Nanbu. Section IV is for general discussion and concluding remarks.

II. GENERALIZED HYDRODYNAMIC EQUATIONS

A. General forms of evolution equations

The modified moment method[3] of solution for the Boltzmann and generalized Boltzmann equation provides the following set[7] of hydrodynamic equations within the framework of 13 moments:

$$\frac{\partial}{\partial t}\rho(\vec{r},t)=-\vec{\nabla}\cdot\rho\vec{u}(\vec{r},t)\ , \tag{2.1}$$

$$\rho\frac{d}{dt}\vec{u}(\vec{r},t)=-\vec{\nabla}\cdot\overleftrightarrow{P}(\vec{r},t)\ , \tag{2.2}$$

$$\rho\frac{d}{dt}\mathcal{E}(\vec{r},t)=-\vec{\nabla}\cdot\vec{Q}(\vec{r},t)-\overleftrightarrow{P}:\vec{\nabla}\cdot\vec{u}\ , \tag{2.3}$$

$$\rho\frac{d}{dt}\hat{\mathbf{P}}(\vec{r},t)=2p\overleftrightarrow{\gamma}+2\rho[\hat{\mathbf{P}}\cdot\overleftrightarrow{\gamma}]^{(2)}-\rho[\overleftrightarrow{\omega},\hat{\mathbf{P}}]-\frac{p\rho\hat{\mathbf{P}}}{\eta_0}\frac{\sinh\kappa}{\kappa}\ , \tag{2.4}$$

$$\rho\frac{d}{dt}\hat{\mathbf{Q}}(\vec{r},t)=(\vec{\nabla}\cdot\overleftrightarrow{P})\cdot\hat{\mathbf{P}}+\vec{Q}\cdot\overleftrightarrow{\gamma}-\hat{C}_p\overleftrightarrow{P}\cdot\vec{\nabla}T-\rho[\overleftrightarrow{\omega},\hat{\mathbf{Q}}]-\frac{T\hat{C}_p p\rho\hat{\mathbf{Q}}}{\lambda_0}\frac{\sinh\kappa}{\kappa}\ , \tag{2.5}$$

$$\rho\frac{d}{dt}\hat{\Delta}(\vec{r},t)=\tfrac{2}{3}\rho\hat{\mathbf{P}}:\overleftrightarrow{\gamma}-\tfrac{2}{3}\rho\hat{\Delta}\vec{\nabla}\cdot\vec{u}-p\frac{d}{dt}\ln(pv^{5/3})-\frac{p\rho\hat{\Delta}}{\eta_{b0}}\frac{\sinh\kappa}{\kappa}\ , \tag{2.6}$$

where the flux evolution equations are in the Jaumann derivative form whose kinetic theory basis is discussed in Refs. 8 and 9. The symbols in (2.1)–(2.6) are defined below:

$$\frac{d}{dt}=\frac{\partial}{\partial t}+\vec{u}\cdot\vec{\nabla}\ ,$$

ρ is the mass density ($v=1/\rho$, specific volume), $\vec{u}$ is the fluid velocity, $\mathcal{E}$ is the internal energy, $\hat{C}_p$ is the specific-heat density at constant pressure, $\overleftrightarrow{P}$ is the stress tensor, $\vec{Q}$ is the heat flux, p is the hydrostatic pressure,

$$\overleftrightarrow{\gamma}=-\tfrac{1}{2}[\vec{\nabla}\cdot\vec{u}+(\vec{\nabla}\cdot\vec{u})^t]+\tfrac{1}{3}\overleftrightarrow{U}\,\mathrm{tr}\overleftrightarrow{P}\ ,$$

$$\overleftrightarrow{\omega}=\tfrac{1}{2}[\vec{\nabla}\cdot\vec{u}-(\vec{\nabla}\cdot\vec{u})^t]\ ,$$

$$\hat{\mathbf{P}}=[\tfrac{1}{2}(\overleftrightarrow{P}+\overleftrightarrow{P}^t)-\tfrac{1}{3}\overleftrightarrow{U}\,\mathrm{tr}\overleftrightarrow{P}]/\rho\equiv[\overleftrightarrow{P}]^{(2)}/\rho\ ,$$

$$\hat{\Delta}=(\tfrac{1}{3}\mathrm{tr}\overleftrightarrow{P}-p)/\rho\ ,$$

$$\hat{\mathbf{Q}}=\vec{Q}/\rho,\quad [\overleftrightarrow{\omega},A]=\overleftrightarrow{\omega}\cdot A-A\cdot\overleftrightarrow{\omega}\ ,$$

η_0 is the Newtonian (Chapman-Enskog) viscosity, λ_0 is the Fourier (Chapman-Enskog) thermal conductivity, η_{b0} is the bulk viscosity,

$$\kappa=\rho[(\tau_p/2\eta_0)^2\hat{\mathbf{P}}:\hat{\mathbf{P}}+(\tau_b/\eta_{b0})^2\hat{\Delta}^2+(\tau_q/\lambda_0)^2\hat{\mathbf{Q}}\cdot\hat{\mathbf{Q}}]^{1/2}\ ,$$

$$\tau_p=[2\eta_0(m_r k_B T/2)^{1/2}]^{1/2}/nk_BT\sigma\ ,$$

$$\tau_b=[\eta_{b0}(m_r k_B T/2)^{1/2}]^{1/2}/nk_BT\sigma\ ,$$

$$\tau_q=[\lambda_0(m_r k_B T/2)^{1/2}]^{1/2}/nk_BT\sigma\ ,$$

m_r is the reduced mass, n is the number density, σ is the size parameter of the molecule, k_B is the Boltzmann constant, and $\overleftrightarrow{U}$ is the unit second rank tensor.

The first three equations (2.1)–(2.3) are mass, momentum, and energy conservation equations, and the last three equations are the evolution equations for the traceless symmetric part $\rho\hat{\mathbf{P}}$ and the excess trace $\rho\hat{\Delta}$ of the stress tensor $\overleftrightarrow{P}$ and for the heat flux $\vec{Q}$. These evolution equations are the constitutive equations for the substance of interest. We have cast them in the Jaumann derivative form which is required of constitutive equations corotational with the frame of reference. The difference between the corotational and fixed frame constitutive equations is in the sign of the rotational terms $\rho[\overleftrightarrow{\omega},\hat{\mathbf{P}}]$ and $\rho[\overleftrightarrow{\omega},\hat{\mathbf{Q}}]$ which take on a negative sign in the case of the corotational formulation. The kinetic theory foundation of corotational formulation is given for constitutive equations in Ref. 9. This sign change has an important significance since otherwise the constitutive equations do not behave correctly as will be pointed out later at a more appropriate point. The kinetic equations such as the Boltzmann equation for dilute gases and the generalized Boltzmann equation for dense fluids yield constitutive equations containing higher-order moments. The latter are neglected in (2.4)–(2.6) since the number of moments is limited to 13 in the present theory. Moreover, because of the nature of the problem the rotational terms $\rho[\overleftrightarrow{\omega},\hat{\mathbf{P}}]$ and $\rho[\overleftrightarrow{\omega},\hat{\mathbf{Q}}]$ do not appear in the evolution equations (1) and (2) in Ref. 1.

The last terms in (2.4)–(2.6) involving the hyperbolic sine function are intimately associated with the entropy production which arises because there are present various fluxes such as heat flux and stress tensor (momentum flux). In fact, we have the entropy production[7]

$$\sigma_{\mathrm{ent}}=k_B g^{-1}\kappa\sinh\kappa\ , \tag{2.7}$$

where

$$g=(m_r/2k_BT)^{1/2}/(n\sigma)^2\ .$$

If the fluxes are small in magnitude, then κ is accordingly small and the entropy production (2.7) may be approximated by

$$\sigma_{\mathrm{ent}}=k_B g^{-1}\kappa^2\ , \tag{2.8}$$

which is simply equal to the Rayleigh-Onsager dissipation function. In the sense that the Rayleigh-Onsager dissipation function holds for linear irreversible processes and the latter occur near equilibrium, the irreversible processes represented by (2.4)–(2.6) may then be said to occur far from equilibrium since the Rayleigh-Onsager dissipation function in (2.8) is a small flux approximation of the entropy production in (2.7).

In the case of a fluid with no bulk viscosity we may set $\hat{\Delta}=0$. It is then necessary to consider only (2.4) and (2.5) for the constitutive equations for the system since it is possible to replace[10] (2.6) with the ideal-gas equation of state especially for steady-state problems. Since we are considering such a case the set of hydrodynamic equations consists of (2.1)–(2.5) in the present study. Since in the present work we are interested in the steady-state problem, we will set the time derivatives of the macroscopic variables in (2.1)–(2.5) equal to zero.

The system of interest here is a Lennard-Jones fluid contained between two infinite concentric cylinders with radius R_i and R_0, respectively; see Fig. 1. The temperatures of the inner and outer cylinders are, respectively, T_i and T_0. The inner cylinder rotates at an angular velocity Ω while the outer cylinder is at rest. In some experiments the outer cylinder is also made to rotate in the opposite direction, but it does not basically change the analysis. The most convenient coordinates for the geometry of the system in hand are the cylindrical coordinates.

B. Steady evolution equations in cylindrical coordinates

The macroscopic variables are then generally functions of r, θ and z. We write various macroscopic variables in components,

$$\rho=\rho(r,\theta,z),\mathscr{E}=\mathscr{E}(r,\theta,z) ,$$

$$\vec{u}=u_r(r,\theta,z)\boldsymbol{\delta}_r+u_\theta(r,\theta,z)\boldsymbol{\delta}_\theta+u_z(r,\theta,z)\boldsymbol{\delta}_z ,$$

$$\begin{aligned}\rho\hat{\mathbf{P}}\equiv\vec{\vec{\Pi}}\equiv{}&\Pi_{rr}\boldsymbol{\delta}_r\boldsymbol{\delta}_r+\Pi_{r\theta}\boldsymbol{\delta}_r\boldsymbol{\delta}_\theta+\Pi_{rz}\boldsymbol{\delta}_r\boldsymbol{\delta}_z\\&+\Pi_{\theta r}\boldsymbol{\delta}_\theta\boldsymbol{\delta}_r+\Pi_{\theta\theta}\boldsymbol{\delta}_\theta\boldsymbol{\delta}_\theta+\Pi_{\theta z}\boldsymbol{\delta}_\theta\boldsymbol{\delta}_z\\&+\Pi_{zr}\boldsymbol{\delta}_z\boldsymbol{\delta}_r+\Pi_{z\theta}\boldsymbol{\delta}_z\boldsymbol{\delta}_\theta+\Pi_{zz}\boldsymbol{\delta}_z\boldsymbol{\delta}_z ,\end{aligned}$$

$$\mathbf{Q}=Q_r(r,\theta,z)\boldsymbol{\delta}_r+Q_\theta(r,\theta,z)\boldsymbol{\delta}_\theta+Q_z(r,\theta,z)\boldsymbol{\delta}_z ,$$

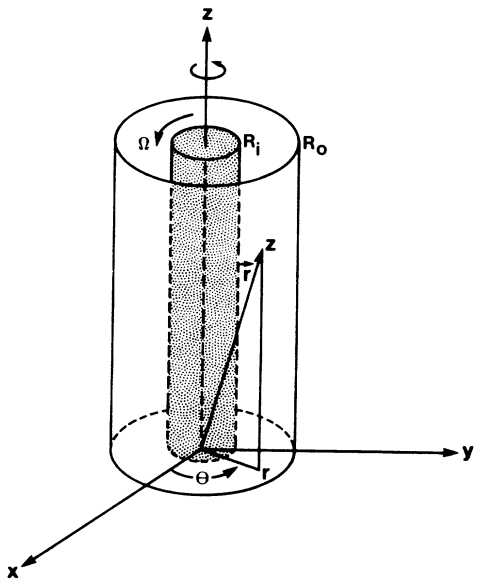

FIG. 1. Coordinates in the cylindrical Couette flow geometry.

where $\boldsymbol{\delta}_r$, $\boldsymbol{\delta}_\theta$, and $\boldsymbol{\delta}_z$ are the orthogonal unit vectors in the cylindrical coordinate system, and the tensor components Π_{rr}, etc. are functions of r, θ, and z.

Because of the assumption of infinite cylinders, there is translational symmetry along the z axis. Consequently, the fluid properties are translationally invariant in z and the macroscopic variables would not depend on z. Since there is also rotational symmetry with respect to the azimuthal angle θ, they are also independent of θ as well. In other words, the macroscopic variables are functions of r only. Taking the symmetry properties into account, we find the steady-state equations for (2.1)–(2.5) in cylindrical coordinates as follows:

$$\frac{d}{dr}(r\rho u_r)=0 , \tag{2.9}$$

$$\rho\left[u_r\frac{du_r}{dr}-\frac{u_\theta^2}{r}\right]=-\frac{d}{dr}(p+\Pi_{rr})-\frac{\Pi_{rr}-\Pi_{\theta\theta}}{r} , \tag{2.10a}$$

$$\rho\left[u_r\frac{du_\theta}{dr}+\frac{u_ru_\theta}{r}\right]=-\frac{1}{r^2}\frac{d}{dr}(r^2\Pi_{r\theta})+\frac{\Pi_{r\theta}-\Pi_{\theta r}}{r} , \tag{2.10b}$$

$$\rho u_r\frac{du_z}{dr}=-\frac{1}{r}\frac{d}{dr}(r\Pi_{rz}) , \tag{2.10c}$$

$$\begin{aligned}\rho u_r\frac{d\mathscr{E}}{dr}=&-\frac{1}{r}\frac{d}{dr}rQ_r-\Pi_{\theta r}\frac{du_\theta}{dr}-\Pi_{zr}\frac{du_z}{dr}\\&+\frac{\Pi_{r\theta}u_\theta-(p+\Pi_{\theta\theta})u_r}{r} ,\end{aligned} \tag{2.11}$$

$$\frac{p\Pi_{rr}}{\eta_0}q_e=-(\tfrac{8}{3}\gamma\Pi_{r\theta}+\tfrac{4}{3}\beta\Pi_{\theta z}) , \tag{2.12a}$$

$$\frac{p\Pi_{r\theta}}{\eta_0}q_e=-2p\gamma-(2\gamma\Pi_{\theta\theta}+\beta\Pi_{\theta z}) , \tag{2.12b}$$

$$\frac{p\Pi_{\theta\theta}}{\eta_0}q_e=\frac{4\gamma}{3}\Pi_{r\theta}-\tfrac{4}{3}\beta\Pi_{zr} , \tag{2.12c}$$

$$\frac{p\Pi_{rz}}{\eta_0}q_e=-2\gamma\Pi_{\theta z}-2\beta\Pi_{zz} , \tag{2.12d}$$

$$\frac{p\Pi_{\theta z}}{\eta_0}q_e=0 , \tag{2.12e}$$

$$\frac{p\Pi_{zz}}{\eta_0}q_e=\tfrac{4}{3}\gamma\Pi_{r\theta}+\tfrac{8}{3}\beta\Pi_{zr} , \tag{2.12f}$$

$$Q_r q_e = -\lambda_0 \chi - (\lambda_0/\alpha)\left[(2\gamma+\omega)Q_\theta + \left[T\hat{C}_p\chi - \frac{u_\theta^2}{r}\right]\Pi_{rr} + 3\beta Q_z\right], \tag{2.13a}$$

$$Q_\theta q_e = -(\lambda_0/\alpha)\left[T\hat{C}_p\chi - \frac{u_\theta^2}{r}\right]\Pi_{\theta r} + (\lambda_0/\alpha)\omega Q_r, \tag{2.13b}$$

$$Q_z q_e = -(\lambda_0/\alpha)\left[T\hat{C}_p\chi - \frac{u_\theta^2}{r}\right]\Pi_{rz} - (\lambda_0/\alpha)(Q_r - 2Q_z)\beta, \tag{2.13c}$$

where

$$\beta = \frac{1}{2}\frac{du_z}{dr},\quad \gamma = \frac{r}{2}\frac{d}{dr}(u_\theta/r),$$
$$\omega = (2r)^{-1}\frac{d}{dr}(ru_\theta),\quad \chi = \frac{d}{dr}\ln T, \tag{2.14}$$
$$\alpha = T\hat{C}_p p,\quad q_e = (\sinh\kappa)/\kappa .$$

The symbol γ represents the shear rate and ω the rotation frequency. It is useful to note the following identity:

$$\omega - \frac{u_\theta}{r} = \gamma$$

so that, for example,

$$\tfrac{1}{3}\gamma + \omega - \frac{u_\theta}{r} = \tfrac{4}{3}\gamma,$$
$$\tfrac{1}{3}\gamma - \omega + \frac{u_\theta}{r} = -\tfrac{2}{3}\gamma,$$

etc. These identities appear in the evolution equations for Π_{rr}, etc. and Q_r, etc. It is also useful to remark that if the heat flux were absent, the constitutive equations (2.12a)–(2.12f) would not involve the rotation frequency ω as is required by the principle[11] due to Stokes on the form of stress tensors for isotropic systems; that is, the stress tensor must be a function of γ only, if the system is isotropic. In this connection it is important to observe that if the Jaumann derivative were not used, i.e., if the sign of the rotational term $\rho[\overleftrightarrow{\omega},\hat{\mathbf{P}}]$ in (2.4) were not negative, then the constitutive equations would have involved ω in contradiction to the Stokes principle, and this fact appears to reinforce the plausibility of the constitutive equation (2.4). We, however, notice that since (2.13b) for Q_θ includes a term depending on ω and the heat flux is coupled to the stress tensor, if the heat flux is present as would be in a more general situation, then the stress tensor components would eventually depend on ω as well through heat fluxes appearing in q_e. Nevertheless, in the absence of the thermoviscous effects the stress tensor evolution equations conform to the Stokes principle. Note that there is no question of isotropy if there is a vectorial process involved, and a heat flux is a vector.

Equation (2.9) integrates trivially to give

$$r\rho u_r = \text{const} . \tag{2.15}$$

Since $u_r = 0$ at the boundaries, the integration constant must be equal to zero and we conclude

$$u_r = 0 \text{ everywhere} . \tag{2.16}$$

This makes all the terms containing u_r in the set (2.9)–(2.14) vanish. This condition also makes (du_z/dr) indeterminate, but at the steady state there should not be nonvanishing u_z on physical grounds. Thus we take

$$u_z = 0,\quad du_z/dr = 0 \text{ everywhere} . \tag{2.17}$$

That is, $\beta = 0$ everywhere. The conditions (2.17) and (2.12e) lead to

$$\Pi_{z\theta} = \Pi_{\theta z} = \Pi_{rz} = \Pi_{zr} = 0,\quad Q_z = 0 . \tag{2.18}$$

It is also convenient to define the normal stress differences N_1 and N_2 as follows:

$$N_1 = \Pi_{\theta\theta} - \Pi_{rr},\quad N_2 = \Pi_{rr} - \Pi_{zz} . \tag{2.19}$$

We will work in terms of normal stress differences instead of the normal stresses themselves.

C. Reduced hydrodynamic equations

It is useful to cast the equations in reduced form by introducing suitable reduced variables. We therefore define the following reduced variables scaled by a suitably chosen set of reference variables. With the definitions

$$\Delta = T_0 - T_i,\quad D = R_0 - R_i$$

and denoting the reference set of variables by T_r, p_r, ρ_r, U_r, η_r, and λ_r for temperature, pressure, mass density, velocity, viscosity, and heat conductivity, respectively, we define the reduced variables

$$T^* = T/T_r,\quad p^* = p/p_r ,$$
$$u^* = u_\theta/U_r,\quad \rho^* = \rho/\rho_r,\quad \xi = r/D ,$$
$$h^* = T\hat{C}_p/T_r\hat{C}_p(T_r),\quad \alpha^* = pT\hat{C}_p/p_r T_r\hat{C}_p(T_r) ,$$
$$\eta^* = \eta_0/\eta_r,\quad \lambda^* = \lambda_0/\lambda_r ,$$
$$\gamma^* = \gamma/(U_r/D),\quad \chi^* = \chi D ,$$
$$\omega^* = \omega/(U_r/D),\quad \Pi^* = \Pi_{r\theta}/(2\eta_r U_r/D) ,$$
$$Q^* = Q_r/(\lambda_r\Delta/DT_r) ,$$
$$N_i^* = N_i/(2\eta_r U_r/D)\quad (i=1,2) ,$$
$$Q_\theta^* = Q_\theta/(\lambda_r\Delta/DT_r) .$$

We will specify more explicitly the reference set of variables later when we perform numerical analysis. It is convenient to introduce the following dimensionless numbers well known in fluid dynamics:

$$M=U_r/(\gamma_0 RT_r)^{1/2},$$

$$\gamma_0=\hat{C}_p/\hat{C}_v,\ R=\text{ gas constant per unit mass},$$

$$R_e=\rho_r U_r D/\eta_r,$$

$$E=U_r^2/\hat{C}_p\Delta\ ,\hat{C}_p=\hat{C}_p(T_r)$$

$$P_r=\hat{C}_p\eta_r T_r/\lambda_r,$$

$$K_n=l/D,\ l=\text{mean-free path}.$$

Here M is the Mach number, R_e is the Reynolds number, E is the Eckert number, P_r is the Prandtl number, and K_n is the Knudsen number. Since the dimensionless numbers above appear in a product form, we will find it convenient to define the following composite reduced numbers:

$$\delta\equiv(2\gamma_0/\pi)^{1/2}MK_n,\ \epsilon\equiv\Delta/4T_rEP_r\ . \tag{2.20}$$

It will be occasionally useful to recall that the normal stresses are second-order quantities.

By collecting the various results above and using the reduced variables defined, we finally obtain the following reduced generalized hydrodynamic equations:

$$\gamma_0M^2\frac{\rho^*u^{*2}}{\xi}=\frac{d}{d\xi}[p^*+\tfrac{2}{3}\delta(N_2^*-N_1^*)]-2\delta N_1^*/\xi\ , \tag{2.21a}$$

$$\frac{d}{d\xi}(\xi^2\Pi^*)=0\ , \tag{2.21b}$$

$$\frac{1}{\xi}\frac{d}{d\xi}(\xi Q^*)+4P_rE\gamma^*\Pi^*=0\ , \tag{2.22}$$

$$\Pi^*q_e=-\eta^*\gamma^*-\tfrac{2}{3}\delta(\eta^*\gamma^*/p^*)(2N_1^*+N_2^*)\ , \tag{2.23a}$$

$$N_1^*q_e=4\delta(\eta^*\gamma^*/p^*)\Pi^*\ , \tag{2.23b}$$

$$N_2^*q_e=-4\delta(\eta^*\gamma^*/p^*)\Pi^*\ , \tag{2.23c}$$

$$Q^*q_e=-\lambda^*\chi^*-(\delta/P_r)(\lambda^*/\alpha^*)\times\left[(2\gamma^*+\omega^*)Q_\theta^*+\tfrac{4}{3}P_r\left[h^*\chi^*-E\frac{u^{*2}}{\xi}\right](N_2^*-N_1^*)\right]\ , \tag{2.24a}$$

$$Q_\theta^*q_e=-(\delta/P_r)(\lambda^*/\alpha^*)\times\left[2P_r\left[h^*\chi^*-E\frac{u^{*2}}{\xi}\right]\Pi^*-\omega^*Q^*\right]\ , \tag{2.24b}$$

where

$$q_e=\sinh\kappa/\kappa\ ,$$

with

$$\kappa=\delta\kappa^*\ ,$$

$$\kappa^*=(\pi^{3/2}/\gamma_0)^{1/2}(T^{*1/4}/\eta^{*1/2}p^*)\times[\Pi^{*2}+\tfrac{1}{3}(N_1^{*2}+N_2^{*2}+N_1^*N_2^*)+\epsilon(\eta^*/\lambda^*)(Q^{*2}+Q_\theta^{*2})]^{1/2}\ .$$

The parameter δ tends to zero as the fluid density increases since in that case K_n tends to zero. Thus in the limit of $\delta\to0$ the set of equations (2.21)–(2.24) reduces to the following set:

$$\gamma_0M^2\frac{\rho^*u^{*2}}{\xi}=\frac{dp^*}{d\xi},\ \frac{d}{d\xi}(\xi^2\Pi^*)=0\ ,$$
$$\frac{1}{\xi}\frac{d}{d\xi}(\xi Q^*)+4P_rE\gamma^*\Pi^*=0\ , \tag{2.23a'}$$

$$\Pi^*=-\eta^*\gamma^*,\ N_1^*=0,N_2^*=0\ ,$$
$$Q^*=-\lambda^*\chi^*,\ Q_\theta^*=0\ . \tag{2.24a'}$$

In fact, this set is exactly the set we obtain from the Navier-Stokes and Fourier equations. We will see that this limit is indeed attained by the numerical result obtained for the density profile; see Fig. 2. Here we note that the Reynolds number R_e is related to the Mach and Knudsen number as follows:

$$R_e=(\pi\gamma_0/2)^{1/2}M/K_n\ .$$

D. Reduced governing equations for the problem

It is known that transport coefficients are density dependent even in the low-density regime. There is evidence that they also depend on thermodynamic gradients. To reflect these facts in the theory, it is necessary to use effective transport coefficients which have such features incorporated into them. This means that we abandon the Chapman-Enskog first approximation formulas for the transport coefficients. This aim can be achieved if we modify the constitutive equations (2.23a') and (2.24a') so that the viscosity and thermal conductivity depend on density and thermodynamic gradients. Attempts[12] have been made in the past to include the higher-order Chapman-Enskog solutions, i.e., the Burnett solutions, in the transport coefficients. However, in such approaches there are some difficult problems since additional boundary conditions are required which are not known, and the constitutive equations are not assured to satisfy the second law of thermodynamics owing to the fact that some Burnett terms make the fluxes inconsistent with the H theorem. We therefore avoid such approaches. In the present study we propose to use the following hydrodynamic equations with such effective transport coefficients:

$$\gamma_0M^2\frac{\rho^*u^{*2}}{\xi}=\frac{dp^*}{d\xi}\ , \tag{2.25a}$$

$$\frac{d}{d\xi}(\xi^2\Pi^*)=0\ , \tag{2.25b}$$

$$\frac{1}{\xi}\frac{d}{d\xi}(\xi Q^*)+4P_rE\gamma^*\Pi^*=0\ , \tag{2.26}$$

$$\Pi^* q_e = -\eta^* \gamma^* \ , \tag{2.27}$$

$$Q^* q_e = -\lambda^* \chi^* \ , \tag{2.28}$$

$$N_1^* = N_2^* = Q_\theta^* = 0 \ , \tag{2.29}$$

with

$$\begin{aligned} q_e &= \sinh\kappa/\kappa \quad (\kappa = \delta\kappa^*) \ , \\ \kappa^* &= (\pi^{3/2}/\gamma_0)^{1/2}(T^{*1/4}/\eta^{*1/2}p^*) \\ &\quad \times [\Pi^{*2} + \epsilon(\eta^*/\lambda^*)Q^{*2}]^{1/2} \ . \end{aligned} \tag{2.30}$$

The constitutive equations (2.27) and (2.28) are then simply the non-Newtonian stress equation and the non-Fourier heat flux equation which we have used in the previous studies.[1,2] These equations, and also (2.21)–(2.24), not only do not require more boundary conditions than those required for the classical Navier-Stokes and Fourier equations but also are fully in conformation to the thermodynamic laws as any macroscopic equations should be. We investigate the utility of this set of equations in this work.

The time-dependent flux evolution equations corresponding to (2.27) and (2.28) are nonlinearized versions of the Maxwell equation[13] and the Cattaneo-Vernotte equation,[14] respectively,

$$\rho^* \tau_1 \frac{d}{dt^*} \Pi^* = -p^* \gamma^* - \frac{p^*}{\eta^*} \Pi^* q_e \ , \tag{2.31a}$$

$$\rho^* \tau_2 \frac{d}{dt^*} Q^* = -h^* p^* \chi^* - \frac{h^* p^*}{\lambda^*} Q^* q_e \ , \tag{2.31b}$$

where τ_1 and τ_2 are nondimensional parameters characterizing relaxation times for Π^* and Q^*, respectively. Since they do not appear in the present theory, there is no need to dwell on them here. Clearly, (2.31a) and (2.31b) reduce to (2.27) and (2.28), respectively, in the case of steady states. They also become the Maxwell equation and the Cattaneo-Vernotte equation when $q_e = 1$. Equation (2.31a) has been tested[15] in comparison with experiment and shown to account for available experimental data quite well. Mathematically, retaining the q_e factor in the constitutive equations is equivalent to expanding the evolution equations for fluxes in series of δ and then resumming partially the resulting series to obtain the constitutive equations with the factor q_e. This procedure is not systematic from the rigorous mathematical standpoint, but in view of the fact that the series in δ may not be convergent but merely asymptotic in its nature, the so-called systematic (Chapman-Enskog[16] type) expansion method employing a truncation at an arbitrary order, usually at the leading order, may not be regarded as mathematically rigorous as generally thought by many kinetic theorists. We therefore believe that a semiempirical procedure as we take here is a more effective way of establishing practical constitutive equations by blending kinetic theory, irreversible thermodynamics, and fluid dynamic measurements. We look for the validity of the approach *a posteriori*.

E. Solution procedure

Since the governing equations (2.25)–(2.28) are highly nonlinear, it is not possible to solve them analytically. They, however, can be fairly easily solved by a numerical method. Here we use the shooting method together with the sixth-order Runge-Kutta method. We describe the solution procedure below.

Equations (2.25b) and (2.26) are easily integrated to yield the pair of equations

$$\Pi^* = C_1/\xi^2 \ , \tag{2.32}$$

$$Q^* = 2P_r E(C_2\xi^{-1} - C_1 u^* \xi^{-2}) \ , \tag{2.33}$$

where C_1 and C_2 are integration constants. When these are substituted into κ^*, we find

$$\kappa = \delta(\pi^{3/2}/\gamma_0)^{1/2}(T^{*1/4}/\eta^{*1/2}p^*) \times \left[\frac{C_1^2}{\xi^4} + 4\epsilon(\eta^*/\lambda^*)(P_r E)^2 \left[\frac{C_2}{\xi} - \frac{C_1 u^*}{\xi^2} \right]^2 \right]^{1/2} . \tag{2.34}$$

Therefore q_e now may be regarded as a function of T^*, ρ^*, C_1, C_2, u^*, and ξ. Then Eqs. (2.27) and (2.28) can be regarded as differential equations for u^* and T^* which, on substitution of (2.32)–(2.34), take the forms

$$\frac{d}{d\xi}\left[\frac{u^*}{\xi} \right] = -\frac{2C_1}{\eta^* \xi^3} \frac{\sinh\kappa(\xi)}{\kappa(\xi)} \ , \tag{2.35}$$

$$\frac{dT^*}{d\xi} = -\frac{2P_r E T^*}{\lambda^*} \left[\frac{C_2}{\xi} - \frac{C_1 u^*}{\xi^2} \right] \frac{\sinh\kappa(\xi)}{\kappa(\xi)} \ , \tag{2.36}$$

where $\kappa(\xi)$ is given by (2.34). There now remains the specification of η_0 and λ_0. For these quantities we take the forms provided by Ashurst and Hoover[17] for the Lennard-Jones fluid. These forms were obtained by fitting the molecular dynamics results to analytic forms. They are

$$\begin{aligned} \eta_0 &= [0.171 + 0.0152[1 - 0.5(\bar{\epsilon}/k_B T)^{1/2} + 2\bar{\epsilon}/k_B T] \\ &\quad \times (\exp\{7.02[1 - 0.2(\bar{\epsilon}/k_B T)^{1/2}]\bar{x}\} - 1)] \\ &\quad \times (m\bar{\epsilon})^{1/2}\sigma^{-2}(k_B T/\bar{\epsilon})^{2/3} \ , \end{aligned} \tag{2.37}$$

$$\begin{aligned} \lambda_0 &= \{0.642 + 0.36[\exp(3.76\bar{x}) - 1]\} \\ &\quad \times \sigma^{-2}(\bar{\epsilon}/m)^{1/2}(k_B T/\bar{\epsilon})^{2/3} k_B T \ , \end{aligned} \tag{2.38}$$

where

$$\bar{x}=n\sigma^3(\bar{\epsilon}/k_BT)^{1/4} ,$$

$\bar{\epsilon}$ is the well depth, and m is the mass of the fluid molecule. σ is the Lennard-Jones potential size parameter. At the normal density or below, the exponential factors are practically equal to unity and we have

$$\eta_0=0.171(m\bar{\epsilon})^{1/2}\sigma^{-2}(k_BT/\bar{\epsilon})^{2/3} , \tag{2.37'}$$

$$\lambda_0=0.642\sigma^{-2}(\bar{\epsilon}/m)^{1/2}(k_BT/\bar{\epsilon})^{2/3}k_BT . \tag{2.38'}$$

With these transport coefficients, we now solve (2.25a), (2.35), and (2.36) numerically subject to suitable boundary conditions.

F. Boundary conditions

In addition to the integration constants C_1 and C_2 there are three more integration constants associated with Eqs. (2.25a), (2.35), and (2.36); that is, there are five in all. These are determined by the boundary conditions. The specification of the velocity and temperature at the inner and outer cylinders takes care of four boundary conditions. The choice of the fifth condition is not obvious for the experimental condition of the present problem since neither the pressure nor the density of the fluid is measured at either one of the boundaries (i.e., cylinders). This difficulty arising from the lack of the clear cut boundary value for pressure or density is not inherent to the present theory only, but to other theories such as the Navier-Stokes theory. However, it must be stressed that since such a boundary value must be provided by experiment, the burden must be placed on experiment rather than theory. We note in passing that Lin and Street[12] take the pressure at the inner boundary equal to the mean pressure of the gas. We find this boundary condition unsatisfactory since at the boundary the pressure at the steady state must be different from the mean pressure. It, however, is simple to overcome such a deficiency of the boundary value. Instead of specifying the value of the density (or pressure) at one of the boundaries, we look for another condition which will allow us to determine the fifth integration constant and thus play the role of the boundary condition. To this end we take advantage of the fact that the mass of the fluid between the two cylinders is conserved in time. Therefore the initial (uniform) experimental density value must be equal to the average steady-state density:

$$\rho_0=\langle\rho(r)\rangle\equiv[2\pi(R_0^2-R_i^2)]^{-1}2\pi\int_{R_i}^{R_0}dr\,r\rho(r) , \tag{2.39}$$

where ρ_0 is the initial uniform mass density and $\rho(r)$ is the steady-state mass density. Once the initial density ρ_0 is given, the density profile can be determined subject to (2.39) in a way consistent with all other boundary conditions. Equation (2.39) constitutes the desired fifth condition which makes the problem well posed.

For the velocities and temperatures at the boundaries we impose the boundary conditions:

$$u_\theta=R_i\Omega \text{ and } T=T_i \text{ at } r=R_i \tag{2.40a}$$

and

$$u_\theta=0 \text{ and } T=T_0 \text{ at } r=R_0 . \tag{2.40b}$$

These are the stick boundary conditions which are traditionally considered applicable to gases at or above the normal density. It is a common practice in gas dynamics to take slip boundary conditions as the gas density diminishes. The notion of slip boundary conditions historically stems from the observation that the gas flow appears to slip over the wall over which the gas moves. In this work we show by explicit calculation that the slip boundary conditions are not necessary. To put the notion of slip in a proper perspective and thereby our method indirectly, we would like to briefly go over how the notion of slip has historically evolved.

After Clausius advanced the mean-free-path theory of transport phenomena and Maxwell proposed his kinetic theory of gases, Kundt and Warburg[18] did a set of experiments on viscosity and thermal conductivity of air, hydrogen, and carbon dioxide and discovered that the transport coefficients did not obey the laws predicted by the kinetic theory, and in fact the gases appeared to be slipping over the wall over which they were flowing. This phenomenon did not agree with the kinetic theory then available to them. They therefore proposed formulas for the transport coefficients which are decreasing functions of pressure in contrast to the Clausius-Maxwell prediction[16] that transport coefficients must be independent of pressure or the density of the gas. In an attempt to remove this discrepancy with experiment Maxwell[19] advanced the idea of diffuse and reflective (specular) scattering of gas molecules off the wall and, with an ingenious but debatable method of calculating the velocity in series of the mean-free path, showed that the velocity slips at the wall in proportion to the mean-free path, which is inversely proportional to the density of the gas. Since his work appeared, numerous theorists[20] elaborated on the idea. But since exact results are generally not possible in such theories, one usually ends up with some plausible approximate results which are further saddled with basically unknown parameters in the form of accommodation coefficients.[21] The latter play a role of adjustable parameters because of lack of information on gas-solid interactions and scattering cross sections which researchers have only recently begun to investigate.[22] As mentioned earlier, transport coefficients are generally density and thermodynamic gradient dependent, and the notion of slip seems to be an outcome of an attempt at making a basically limited theoretical result work beyond its limit of validity. The empirical formula for transport coefficients by Kundt and Warburg[18] has already indicated that the first-order Chapman-Enskog formulas are not adequate for the transport coefficients if the density is sufficiently low and the Navier-Stokes equations therefore are not appropriate for description of flow phenomena in such a fluid. The proposition we would like to make in this work is that the transport processes in low-density gases

are basically nonlinear, and slip phenomena observed in the laboratory are a manifestation and consequence of nonlinear transport processes, but the slip boundary conditions are not necessary. It appears sufficient to use the stick boundary conditions, provided the transport processes are appropriately nonlinear. The proposition is substantiated with explicit numerical calculation and comparison with independent results by Nanbu[5] and the Navier-Stokes theory with slip boundary conditions and with experiment.

III. SOLUTION OF THE EQUATIONS AND FLOW PROFILES

Alofs and Springer[4] reported on density profiles of argon in cylindrical Couette flow. To make a comparison of our results with theirs we take the initial density obtained from the reported chamber pressure and temperature in their experiment. The reference temperature is taken to correspond to the mean value of the wall temperatures. Other reference values are also taken to correspond to the experimental condition. Given these reference quantities, various dimensionless parameters such as M, K_n, P_r, E, and the aspect ratio can be determined. The reference transport coefficients η_r and λ_r are η_0 and λ_0 calculated in terms of the reference temperature and density chosen. The solution to (2.25a), (2.35), and (2.36) is obtained, subject to the five reduced boundary conditions

$$u^*=0, \quad T^*=T_0/T_r \quad \text{at } \xi=R_0/D \ ,$$

$$u^*=1, \quad T^*=T_i/T_r \quad \text{at } \xi=R_i/D \ ,$$

and

$$\langle \rho^*(\xi) \rangle = 1 \ ,$$

by using the sixth-order Runge-Kutta numerical scheme and the shooting method. The values of C_1 and C_2 are first guessed together with a value of the pressure (or density) at one of the cylinder walls, and the governing equations are solved in an attempt to satisfy the four boundary conditions and reach an average reduced density equal to unity. This procedure is repeated until an imposed tolerance is satisfied. Since this technique is rather tedious, we have devised a modified Newton-Raphson iterative scheme that would automatically determine the appropriate values of the two constants and pressure (or density) at the boundary.

In order to compare our results with those obtained experimentally we have to use the same values for the dimensionless parameters involved. There is, however, some ambiguity in the way some of the parameters were defined on one hand and in the choice of some reference quantities on the other. The wall temperatures were initially identical, but the wall temperatures at steady state, however, were found to be different by 8 °C. We therefore defined our Mach number on the basis of the mean value of the two steady-state wall temperatures. This latter is then our reference temperature. The Mach number thus calculated turns out to be comparable to that used by Alofs and Springer, i.e., 0.9908 for ours compared to 0.9917. The aspect ratio A, the Eckert and Prandtl numbers are set equal to the experimental conditions, i.e., $A=\frac{2}{3}$, $E=25.115$, and $P_r=0.666$. Note that the specification of the Eckert number fixes that of the temperature ratio T_i/T_0. The Chapman-Enskog transport coefficients are those for a Lennard-Jones gas, while the ones used in the experiment[4] are based on the Maxwellian model for the intermolecular force. For this reason, the K_n values in the present investigation are slightly higher than the values quoted in the paper by Alofs and Springer[4] and by Nanbu[5] although they are both based on the same value of the initial density.

Although the present calculations cover all the flow properties, only the density profiles can be compared with the experimental results since others are experimentally unavailable. In the experiment by Alofs and Springer the initial chamber pressures varied from 0.050 to 0.0020 mm Hg with corresponding Knudsen number ranging from 0.0426 to 1.065. When converted to the

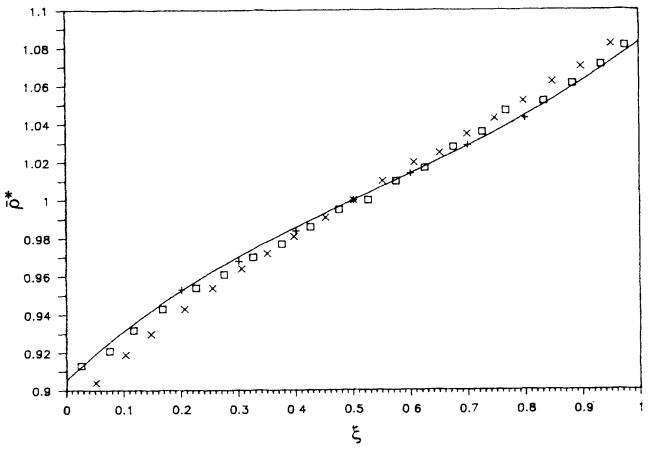

FIG. 2. Reduced density vs reduced distance for $K_n=0.0544$ and $p_0=0.05$ mm Hg. +, experimental value by Alofs and Springer; □, simulation value by Nanbu (Ref. 5); ×, Navier-Stokes theory with slip boundary conditions; ——, the present theory. The reduced distance in this figure and others is defined by $\xi=(r-R_i)/D$.

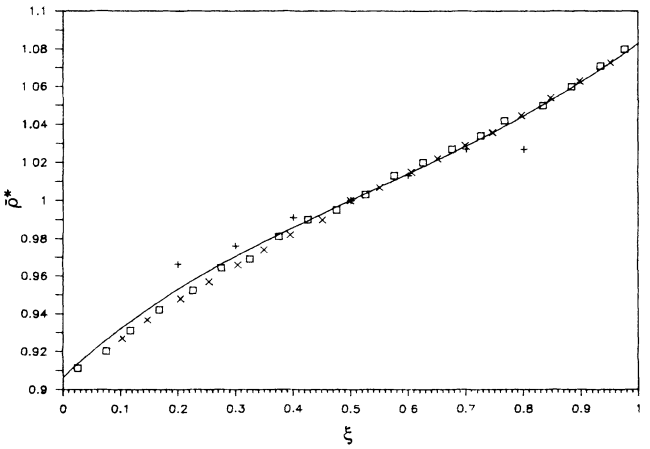

FIG. 3. Reduced density vs distance for $K_n=0.1046$ and $p_0=0.026$ mm Hg. +, experiment; □, simulation; × Navier-Stokes theory; ——, the present theory.

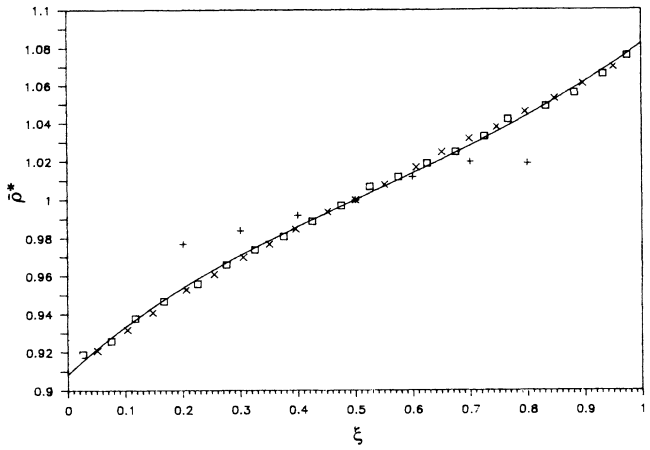

FIG. 4. Reduced density vs reduced distance for $K_n = 0.1388$ and $p_0 = 0.00196$ mm Hg. +, experiment; □, simulation; ×, Navier-Stokes theory; ——, the present theory.

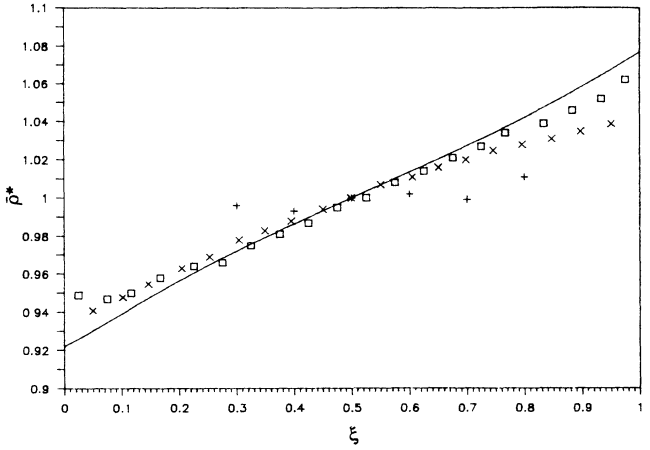

FIG. 6. Reduced density vs reduced distance for $K_n = 0.5184$ and $p_0 = 0.00525$ mm Hg. +, experiment; □, simulation; ×, Navier-Stokes theory; ——, the present theory.

present choice of reference variables, the Knudsen numbers range from 0.0544 to 1.3962.

The density profiles for different initial chamber pressures are shown in Figs. 2–7 where the + symbols represent the experimental data,[4] the squares the simulation results by Nanbu,[5] the symbols × the results by the Navier-Stokes theory with slip boundary conditions, and the solid curve the solutions by the present theory. They are of particular interest since density measurements were mainly the object of attention in the experiment.[4] The corresponding velocity, temperature, and pressure distributions are also plotted in Figs. 8–10 on which we will comment shortly. The profiles obtained by other models are also available in Refs. 4 and 5 to which the reader is referred. For $K_n = 0.0544$, 0.1388, and 0.3201 the present solutions are virtually identical with the simulation results by Nanbu[5] and the results by the Navier-Stokes equations with slip boundary conditions. However, three sets begin to show a qualitative difference from the experimental results as the Knudsen number increases although absolute numerical differences from the experimental values are invariably less than a few percent at most. From $K_n = 0.5184$ up, the simulation profiles show a noticeable minimum in density in the vicinity of the inner-cylinder wall whereas the results by the present theory, i.e., generalized hydrodynamic equations (2.25)–(2.28), show only a rather weak minimum at the Knudsen numbers in question. However, such a minimum appears noticeably at higher Knudsen numbers as is shown in Fig. 11, where density profiles are shown for $K_n = 1.362$, 9.459, and 212.8. The Navier-Stokes results do not show such a minimum at all. Because of limitations on measurements the experiment is not able to determine the presence of such a minimum. The fact that there appears a minimum in the high Knudsen number density profiles by both Monte Carlo and present methods seems to suggest that the two methods share a common physical mechanism of causing the gas to accumulate near the inner wall. A more recent calculation shows that a minimum does not appear if the normal stresses are included. In any case, the numerical differences between the three sets generally do not exceed 5% to 6%. Here we also note that the Navier-Stokes theory results with slip boundary conditions coincide

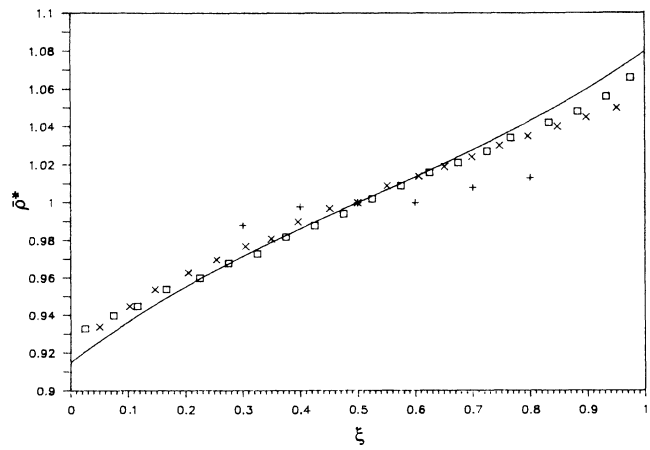

FIG. 5. Reduced density vs reduced distance for $K_n = 0.3201$ and $p_0 = 0.0085$ mm Hg. +, experiment; □, simulation: ×, Navier-Stokes theory; ——, the present theory.

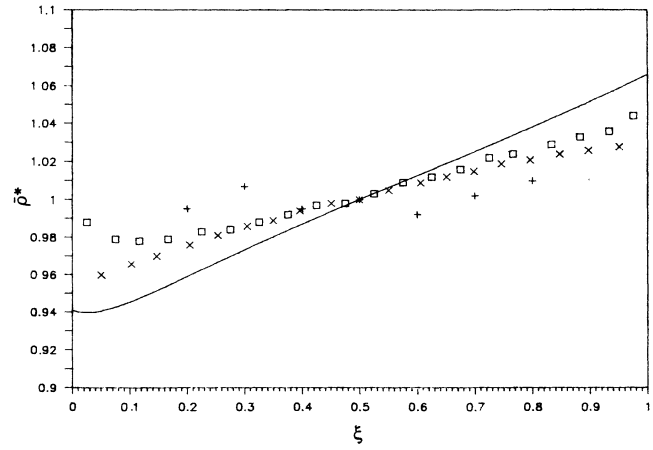

FIG. 7. Reduced density vs reduced distance for $K_n = 1.362$ and $p_0 = 0.009$ mm Hg. +, experiment; □, simulation; ×, Navier-Stokes theory; ——, the present theory.

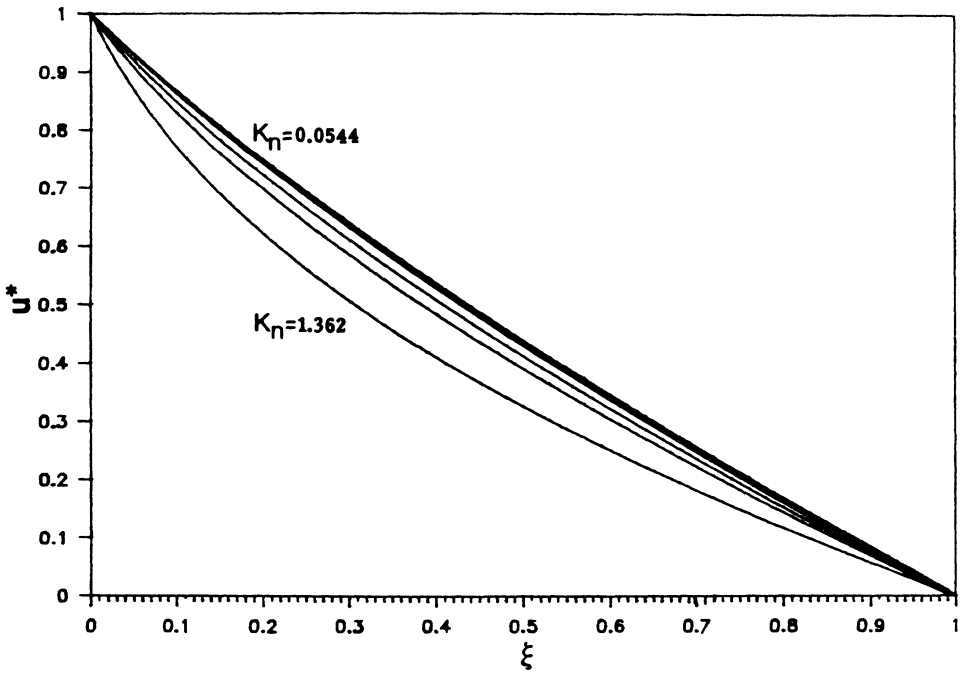

FIG. 8. Reduced velocity profiles for various values of K_n: 0.0544, 0.1046, 0.1388, 0.3201, 0.5184, 1.362. The Knudsen numbers are not indicated for curves between the first and the last for lack of space.

with the Navier-Stokes theory results with stick boundary conditions as the Knudsen number vanishes. Thus the Navier-Stokes theory density profile in Fig. 2 may be regarded as practically the no-slip Navier-Stokes density profile. Since the simulation method itself is by no means exact, it is reasonable to state that *the present nonlinear hydrodynamic equations with stick boundary conditions are able to reproduce the density profiles comparable with the simulation results in most of the range of Knudsen numbers so far studied.* Moreover, it is also possible to conclude that even though there are absent in the present theory the accommodation coefficients which are basically adjustable parameters, the present results are comparable to the results of the Navier-Stokes theory with slip boundary conditions. Therefore the present theory is not only as accurate as the usual hydrodynamic theory em-

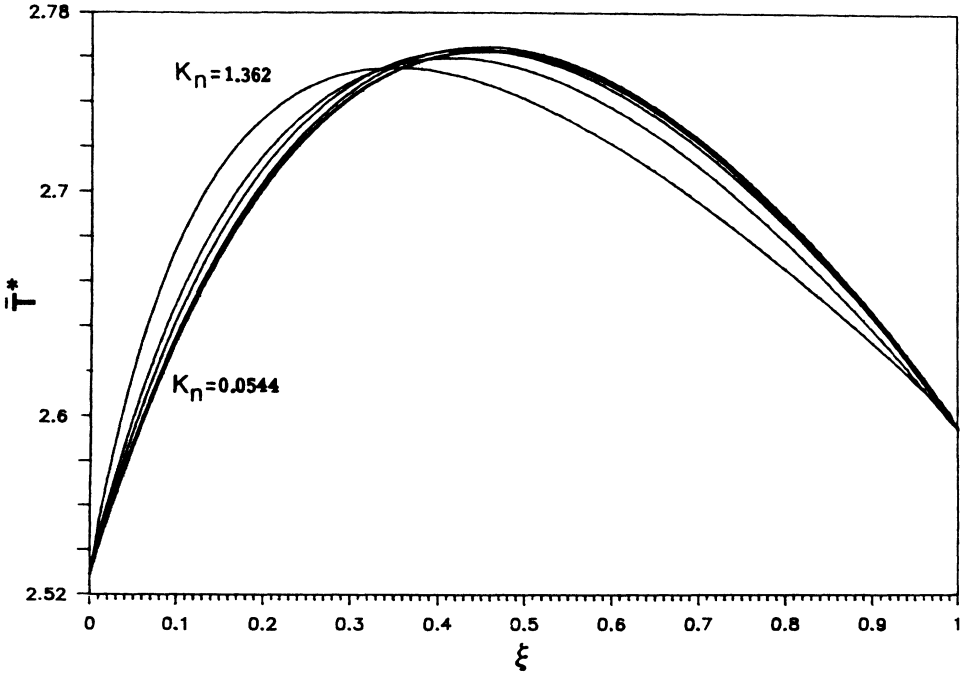

FIG. 9. Reduced temperature profiles for various values of K_n. The values of the Knudsen numbers are the same as in Fig. 8. The reduced temperature $\bar{T}^*$ in this and later figures is defined by $\bar{T}^* = k_B T/\bar{\epsilon}$, where $\bar{\epsilon}/k_B = 119.8$ K (see Ref. 26).

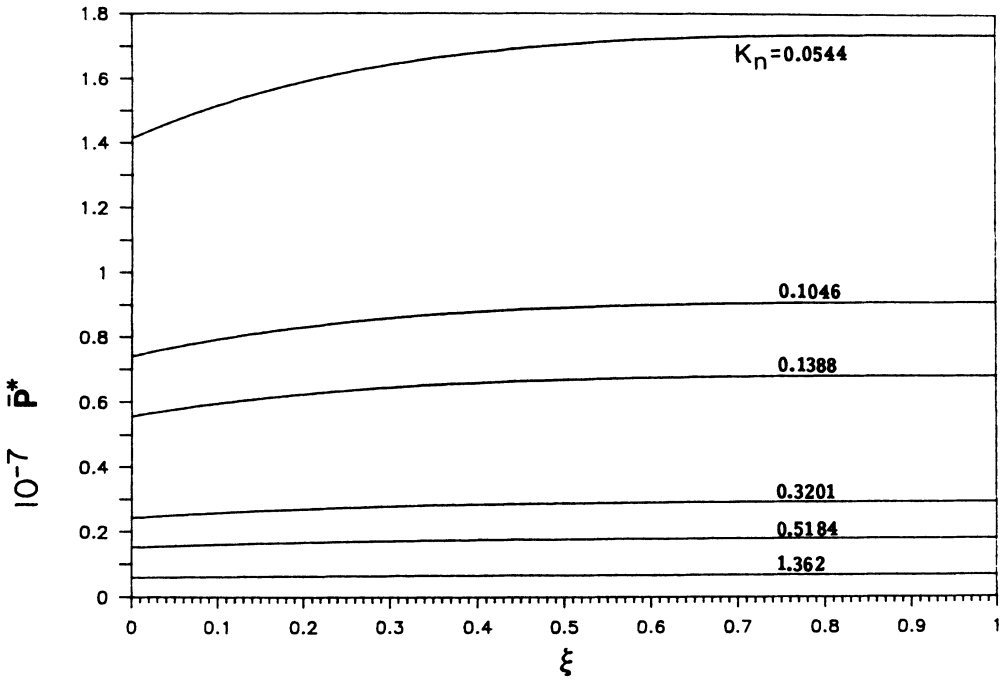

FIG. 10. Reduced pressure profiles for various values of K_n. The reduced pressure $\bar{p}^*$ in this and later figures is defined by $\bar{p}^* = p\sigma^3/\bar{\epsilon}$, where $\sigma = 3.405 \times 10^{-10}$ m (see Ref. 26).

ploying slip boundary conditions, but also simpler than the latter.

The velocity, temperature, and pressure profiles presented in Figs. 8–10 do not exhibit slips as the corresponding profiles obtained by Nanbu[5] do even at the lowest Knudsen number studied. In the present work we instead observe a gradual formation of boundary layer near the inner boundary as K_n increases. The presence of a boundary layer is consistent with the picture provided by kinetic boundary layer theory[6] with which the experiment and simulation density profiles appear to be consistent. In the present theory the boundary layers are due to the nonlinear terms in the constitutive equations for the stress tensor components and heat flux components. The evidence for this view is also supported by the boundary layer calculation reported previously.[23] Since there is no experimental measurement available at present to sort out these conflicting numerical results regarding slips in velocity and temperature, we are not able to draw a definite conclusion at the present time. According to the calculations that include normal stresses which will be reported elsewhere,[24] the lack of slip in the present results is due in part to the neglect of normal stresses. In any case, a thin boundary layer may be easily mistaken for a slip within experimental errors, and we will have to leave the question unresolved for now and reserve it for future study.

In the case of the simulation method it is difficult to have a qualitative guess for the flow behavior on the basis of the governing (in this case the Boltzmann) equation since the Boltzmann equation does not readily reveal the flow characteristics that one can intuitively deduce as in the case of the present generalized hydrodynamic equations or Navier-Stokes equations for that matter. For example, by examining certain limiting flow regimes, one can often be in a position to anticipate the flow behavior without actually having to solve the governing equations, such as the case here in hand where it is possible to predict the flow behavior in the limit of a large Knudsen number. In this limit it is easy to see from (2.30) that the shear stress vanishes with increasing K_n and therefore the equation is reduced to the form

$$\Pi^* = 0$$

since q_e^{-1} vanishes exponentially with increasing K_n at first glance. As a matter of fact, the above equation arises since the shear stress decays at large K_n like $K_n^{-1} \ln K_n$ according to more elaborate analysis.[15] From (2.28) an exactly analogous argument can be established for the behavior of the heat flux Q^* in the limit of a large Knudsen number. In this case the flow does not manifest any ability for momentum transfer or heat conduction; it in fact behaves like an ideal flow. As was mentioned before, (2.25b) and (2.26) are identically satisfied to $O(K_n^{-1} \ln K_n)$, and the only surviving equation is (2.25a) which is nothing but Euler's equation for the present geometry.

Since the density is inversely proportional to K_n the inertia terms, which are proportional to the density, behave like K_n^{-1}, and therefore decay faster than the shear stress or heat flux as K_n gets large. In this case the inertia term in (2.25b) becomes small and the pressure gradient vanishes except near the inner wall. This is clearly indicated in Fig. 10, where the pressure is practically constant for high-K_n values. We then conclude that since inertia effects become insignificant at a large Knudsen number, the fluid will not be entrained by the rotating cylinder

and tend to stagnate at the inner cylinder. Moreover, the gas will tend to accumulate near, and hence acquire the properties of the outer, stationary wall as is clear from the fact that the density value in the vicinity of the outer wall tends to remain larger than near the inner wall, if one examines the density profiles for $K_n = 0.3201$, 0.5184, and 1.362. This is expected owing to the presence of centrifugal forces inducing a pressure gradient which in turn acts on the fluid and "crowds" the gas near the outer wall. On the other hand, although the difference in wall temperatures is not high, viscous energy dissipation is sufficiently generated to cause a tangible temperature rise. This is particularly visible in the vicinity of the inner cylinder where the shear stress is highest, thus inducing a steep temperature rise there; see Fig. 9. Note also that the temperature maximum tends to shift towards the inner cylinder as K_n increases. This indicates that the flow is limited to the neighborhood of the inner cylinder as the gas becomes more and more rarefied. In the cases of relatively large Knudsen numbers (particularly in the case of the initial chamber pressures of 0.005 25 and 0.002 mm Hg), the experimental results show a flattening tendency of the density profile.

In Figs. 11–14 are plotted the density, velocity, temperature, and pressure profiles for $K_n = 1.362$, 9.459, and 212.8. As the Knudsen number increases, the boundary layers become more pronounced in the velocity and temperature profiles while the pressure profiles become flat. This feature is compatible with kinetic boundary layer predictions. The density profile in particular becomes gradually flattened with increasing Knudsen number but not as much as the experimental data indicate. More recent calculations[24] indicate that the generalized hydrodynamic equations (2.25)–(2.28) used here are not sufficient and require the normal stress terms which have been left out to get the set of equations (2.25)–(2.28) from the general set (2.21)–(2.24). The results of the studies indicate that the normal stresses neglected in the present calculation play a very important role in understanding the flow profiles experimentally observed. The results of the studies[24] will be reported in the near future.

IV. DISCUSSION AND CONCLUDING REMARKS

Hydrodynamic equations such as Euler's and Navier-Stokes equations are accorded kinetic theory foundations principally by the Boltzmann kinetic equation and the Chapman-Enskog solution[16] method or Grad's moment method.[20(b)] It is now well known that the first-order solution to the Boltzmann kinetic equation or its variants by the Chapman-Enskog or the Grad method yields the Navier-Stokes and Fourier equations, and the transport coefficients (i.e., viscosity and thermal conductivity) appearing therein are density independent as was originally predicted by Maxwell. The density independence of transport coefficients, however, is a rather confining restriction. Therefore, if the Chapman-Enskog first-order forms for the transport coefficients are used in the classical hydrodynamic equations, the latter are, as is well known, applicable to gases of normal density and relatively close to equilibrium. (It must be stressed that this statement is not applicable to the case of Navier-Stokes and Fourier equations in which density-dependent transport coefficients are empirically used as in many applications). From the standpoint of deriving hydrodynamic equations from kinetic (molecular) theory of fluids the classical hydrodynamic (i.e., Navier-Stokes and Fourier) equations are subject to another limitation: That is, they apply to the bulk of a fluid sufficiently far away from the walls of the container, since the kinetic equations used for such a derivation have no provision for the wall effect since they do not generally take the presence of walls into

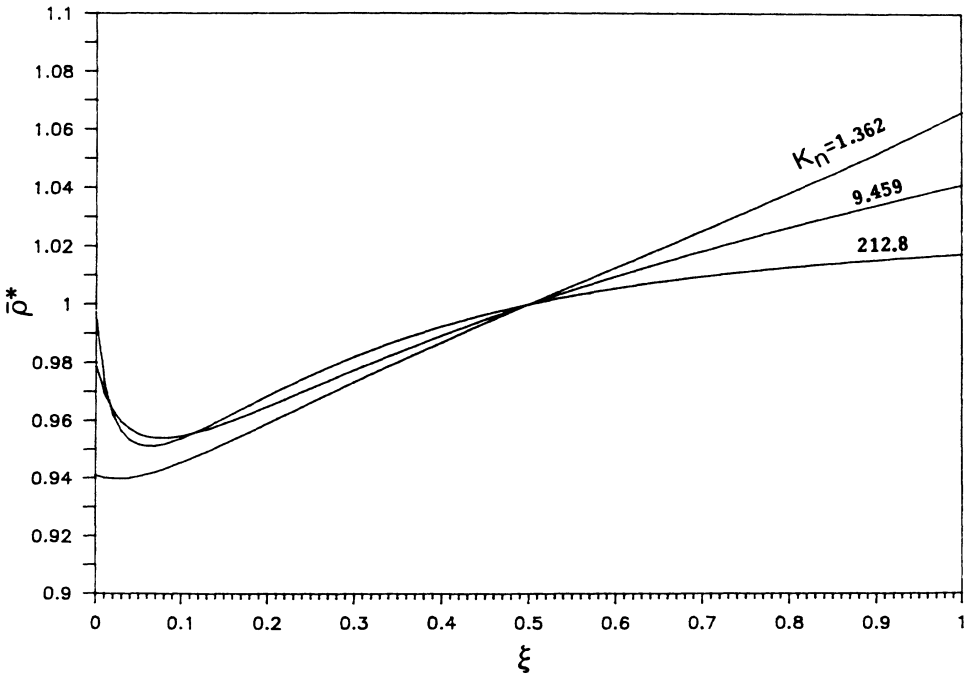

FIG. 11. Reduced density profiles for $K_n = 1.362$, 9.459, 212.8. Note that a minimum appears in the profiles.

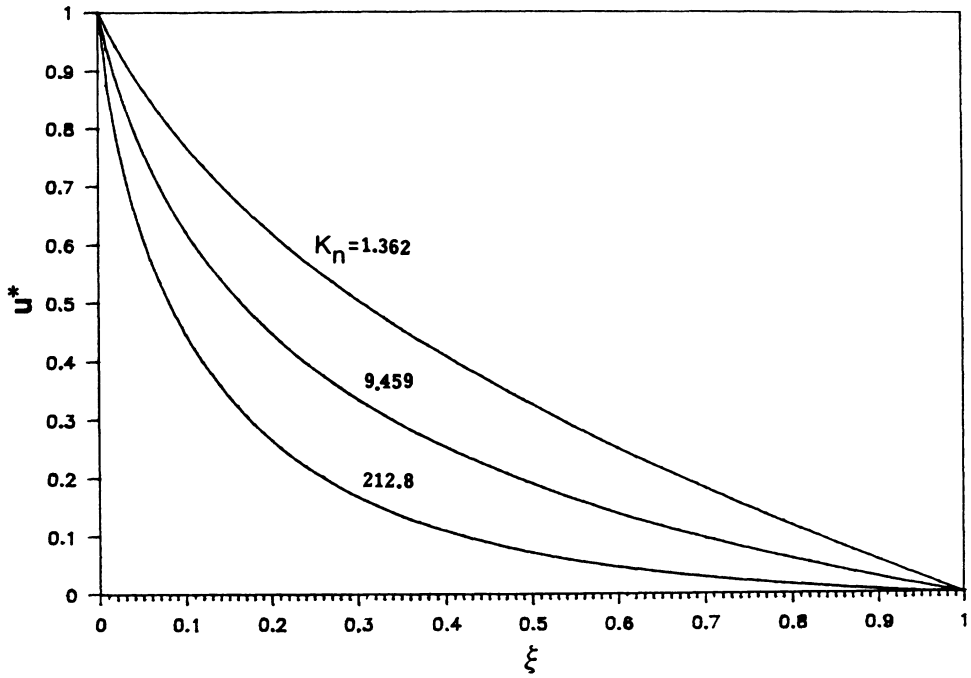

FIG. 12. Reduced velocity profiles for $K_n = 1.362, 9.459, 212.8$.

account. Therefore when we use the hydrodynamic equations without wall effects explicitly built into them, we are making an implicit assumption that the bulk properties of the fluid can be extended all the way to the walls (boundaries) confining the fluid, and the walls do not affect the fluid properties significantly. This assumption is justifiable if the solid-fluid molecule interactions are insignificant for the kind of experimental data in question. At least, it removes in practice a rather difficult, and often intractable, question of interfacial phenomena occurring in the interface between the solid wall and the fluid.

The wall effects are often taken into account by imposing a suitable boundary condition on the distribution functions obeying a kinetic equation, e.g., the Boltzmann equation or its variants. The boundary condition usually consists of a diffusive scattering component made up with an equilibrium distribution function at the temperature of the wall and a specularly reflective scattering component for which the distribution functions are of nonequilibri-

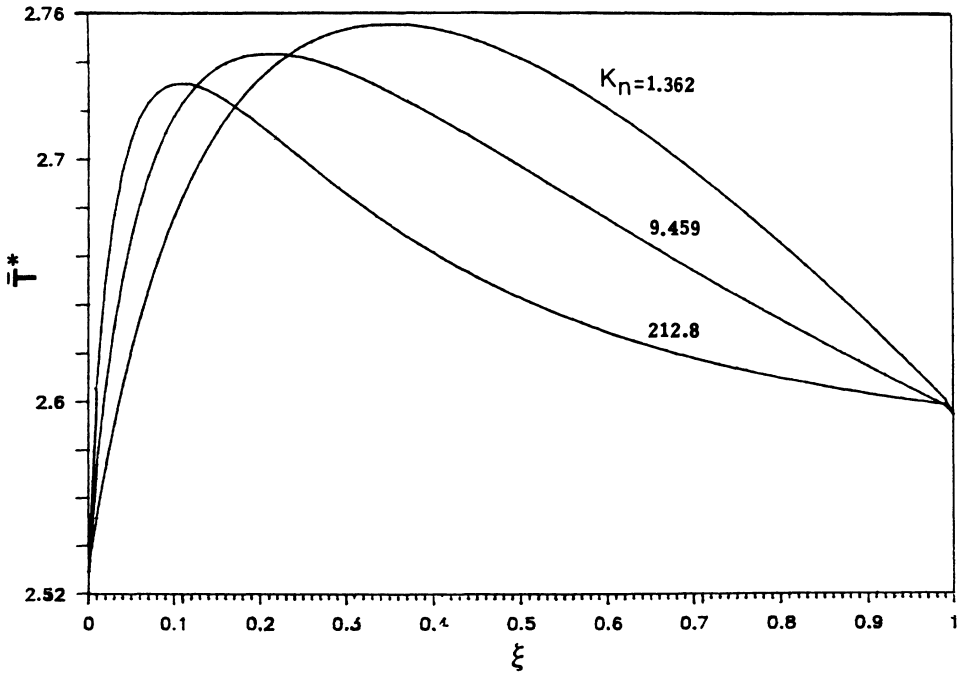

FIG. 13. Reduced temperature profiles for $K_n = 1.362, 9.459, 212.8$.

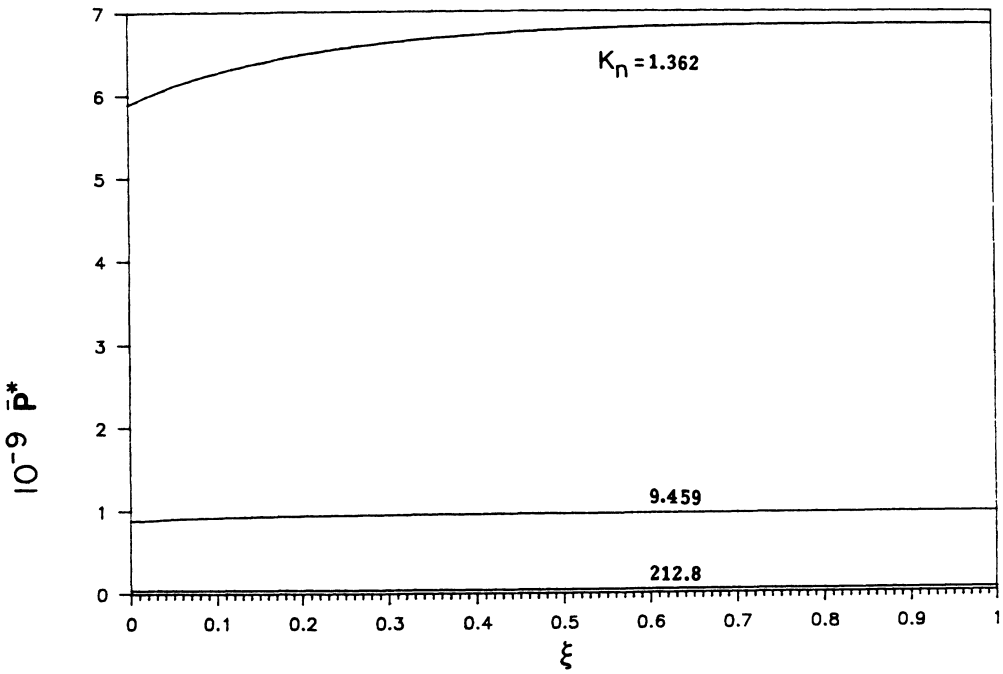

FIG. 14. Reduced pressure profiles for $K_n = 1.362, 9.459, 212.8$.

um and of the bulk gas. The absolute magnitudes of both diffuse and specular contributions are not possible to determine, but their ratio is determined within parameters known as accommodation coefficients which cannot be determined within the framework of the theory. They are basically adjustable parameters that must be suitably chosen to fit experimental data. Instead of using the boundary conditions on the distribution functions at the wall to account for the wall effects, one can include the wall-gas collision effect in the Boltzmann collision integral as in the work by Dorfman and van Beijren.[20(e)] But because of basically the same nature of the collision integral as in the boundary-condition approach, the final results of their theory are not basically different from those by the boundary-condition approach, although there can be some advantages in the theory of Dorfman and van Beijren. Both approaches indicate the boundary conditions on velocity and temperature showing a slip. It is, however, not known if the slip predicted by their theory yields profiles that agree with experiment.

It must be noted that even smooth and clean surfaces attract gas molecules according to an approximate force law:[21] $f = -br^{-4}$, where b is a positive constant related to the van der Waals force constant, and often the gas molecules get adsorbed or even chemisorbed on the surface. They then acquire the temperature of the surface and then get desorbed into the bulk. Even a rarefied gas goes into thermal and mechanical equilibrium with the walls, and heat and momentum transfers between the walls and the gas however rarefied, necessary for such equilibrium, cannot be accounted for without taking into account such intimate interactions causing the gas molecules to equilibrate with the walls. From this molecular viewpoint the slip-boundary-condition approach merely parametrizes such surface phenomena in terms of accommodation coefficients with no gain in molecular picture, on one hand, and ignores the important aspects of nonlinear transport processes which play an important role in determining flow profiles near the boundaries, on the other hand. The present method, by taking stick boundary conditions, presumes equilibrium of the fluid at the boundary with the surface and recognizes the importance of nonlinear transport processes which we believe are important for understanding flow properties of rarefied gases.

As the density decreases, the transport coefficients begin to depend on the density of the gas, but when such density dependence is ignored and the classical hydrodynamic equations are applied to gas-flow problems, glaring discrepancies begin to show up as was observed by Kundt and Warburg[18] for the first time. Maxwell[13] repaired the theory by including the gas-solid interaction in the form of empirical parameters which have now come to be known as accommodation coefficients, but he retained the density-independent transport coefficients. This is an *ad hoc* procedure which later, more refined theories in rarefied gas dynamics have retained in one form or another. A completely satisfactory kinetic theory of rarefied gas dynamics that yields hydrodynamics equations without *ad hoc* parameters such as accommodation coefficients is yet to materialize.

In this work as in the previous papers we have taken the approach in which the transport coefficients are made not only density dependent but also thermodynamic gradient dependent, and the hydrodynamic equations with such coefficients are assumed to be valid all the way to the boundaries where stick boundary conditions are applicable for velocity and temperature. This approach, therefore, is opposite to the one that uses linear density- and gradient-independent transport coefficients together

with slip boundary conditions. With explicit numerical solution of generalized hydrodynamic equations we have shown in this work that the present approach yields sensible results when compared with experiment, the results by the Navier-Stokes theory with slip boundary conditions, and direct simulation results; see Figs. 2–7. Especially, comparison with the simulation results is quite good, thereby rendering support for the approach taken; it is as good as the simulation method as far as comparison with experiment is concerned. Nevertheless, there is considerable room for improvement since there are significant deviations from experiment in the high-Knudsen-number regime.

The present calculations in effect point out the importance of nonlinear constitutive equations for flow properties of a fluid. In this connection it is useful to remark that the transport coefficients depend on shear rate and also on density, such as $n \ln(n^{-1})$, where n is the number density of the gas. Therefore the viscosity diminishes with density as the gas rarefies. Such viscosity formula is shown to give a correct behavior of the boundary layer in a previous work[23] and also account for nonequilibrium molecular dynamics results[15(a),15(c)] on Ar.

The direct simulation method used by Nanbu[5] is based on the simulation method by Bird[25] and is believed to give exact results since it is claimed to solve by a Monte Carlo method the Boltzmann equation without an approximation. If so, the good agreement with the results by the present theory, particularly the minimum in the density profiles in both methods (see Figs. 7 and 11), and the deviations of both results from the experimental values in the high Knudsen numbers raise a question as to why the direct simulation gives results deviating from experiment while agreeing with the results obtained from approximate equations which the generalized hydrodynamic equations in the present paper are. While the particular experiment that has provided the data used for comparison may require refinement, it is also reasonable to think that the direct simulation method itself is more approximate than its practitioners would like to believe. We have made some careful studies of various steps taken in the direct simulation method and have noticed that the so-called decoupling approximation is used which considers the streaming motion of particles as being independent of collision and thus decoupled from the collisional processes involved in evolution of particle motions. There is also a step which locally linearizes the Boltzmann collision integral which is quadratically nonlinear in distribution functions. It appears that the combination of these two approximations makes the evolution equation—the Boltzmann equation—locally linear or quasilinear at best, and the two approximations might be effectively preventing the method from describing the high-Knudsen-number regime of fluid behavior. This view seems to make sense if it is recalled that (2.25)–(2.28) are obtained by neglecting some terms which are not negligible as the Knudsen number increases, and therefore they become increasingly more approximate. We therefore believe that the direct simulation method itself might need refinement with removal of the local linearization of the Boltzmann collision integral first of all.

In conclusion, we have shown in comparison with experiment and the results by a direct simulation method that the nonlinear constitutive equations (2.27) and (2.28) give rise to generalized hydrodynamic equations which, with stick boundary conditions, yield density profiles comparable to those by the direct simulation method in particular although there are significant deviations from the experimental data at high Knudsen numbers. Further improvements in the quality of generalized hydrodynamic equations appear to be necessary. Nevertheless, the present theory shows that studies in gas dynamics and rarefied gas behavior in particular can be made with nonlinear transport coefficients and the conventional stick boundary conditions for the generalized hydrodynamic equations.

ACKNOWLEDGMENT

This work is supported in part by the Natural Sciences and Engineering Research Council of Canada, which is gratefully acknowledged.

---

*Also at the Department of Physics, McGill University, 3600 University Street, Montreal, Quebec, Canada H3A 2T8.

[1]D. K. Bhattacharya and B. C. Eu, Phys. Rev. A **35**, 821 (1987).

[2]B. C. Eu, R. E. Khayat, G. D. Billing, and C. Nyeland, Can. J. Phys. **65**, 1090 (1987).

[3]B. C. Eu, J. Chem. Phys. **73**, 2958 (1980); **74**, 2998 (1981); **74**, 3006 (1981); **80**, 2123 (1984); **82**, 4283 (1985); **74**, 6362 (1981); **87**, 1220 (1987).

[4]D. J. Alofs and G. S. Springer, Phys. Fluids **14**, 298 (1971).

[5]K. Nanbu, Phys. Fluids **27**, 2632 (1984).

[6]M. N. Kogan, *Rarefied Gas Dynamics* (Plenum, New York, 1969).

[7]There are some typographical errors in Ref. 1 which we would like to correct here: The term $-\frac{2}{3}\rho\vec{\nabla}\cdot\vec{u}$ in Eq. (2) of Ref. 1 should read $-\frac{2}{3}\rho\hat{\Delta}\vec{\nabla}\cdot\vec{u}$. Equation (14) in Ref. 1 should read $\kappa_1=\rho[(\tau_p/2\eta_0)^2\hat{\mathbf{P}}:\hat{\mathbf{P}}+(\tau_b/\eta_{b0})^2\hat{\Delta}^2+(\tau_q/\lambda_0)^2\hat{\mathbf{Q}}\cdot\hat{\mathbf{Q}}]^{1/2}$.

[8]G. Jaumann, Sitzungsber. Akad. Wiss. Wien Math. Naturwiss. Kl. Abt. 2A: **120**, 385 (1911); W. Prager, *Introduction to Mechanics of Continua* (Ginn, Boston, 1961).

[9]B. C. Eu, J. Chem. Phys. **82**, 3773 (1985).

[10]This replacement of (2.6) with the ideal-gas equation of state is reasonable only if the nonequilibrium effect, especially the effect of shear, on the pressure is neglected. This effect may not be negligible for some cases and must be included. Then the problem becomes much more involved since the radial and axial components of the velocity cannot vanish at the boundaries and consequently there are a larger number of equations to solve. This aspect will be studied in connection with a non-steady-state problem in the future.

[11]G. G. Stokes, Trans. Cambridge Philos. Soc. **8**, 287

(1844–1849).
[12]T. C. Lin and R. E. Street, National Advisory Committee for Aeronautics Report No. 1175 (1954).
[13]J. C. Maxwell, Philos. Trans. R. Soc. London **A157**, 49 (1867).
[14]C. Cattaneo, C. R. Acad. Sci. Paris **247**, 431 (1958); P. Vernotte, *ibid.* **247**, 3154 (1958).
[15](a) B. C. Eu, J. Chem. Phys. **79**, 2315 (1983); Phys. Lett. **A96**, 29 (1983); (b) Y. G. Ohr and B. C. Eu, *ibid.* **101A**, 338 (1984); J. Chem. Phys. **81**, 2756 (1984); B. C. Eu, *ibid.* **82**, 4683 (1985); (c) D. K. Bhattacharya and B. C. Eu, Phys. Rev. A **35**, 4850 (1987).
[16]S. Chapman and T. G. Cowling, *Mathematical Theory of Non-Uniform Gases,* 3rd ed. (Cambridge, London, 1970).
[17]W. T. Ashurst and W. G. Hoover, Phys. Rev. A **11**, 658 (1975).
[18]A. Kundt and E. Warburg, Philos Mag. **50**, 53 (1875).
[19]J. C. Maxwell, *Collected Works of J. C. Maxwell* (Cambridge University Press, London, 1927), Vol. II, p. 86.
[20](a) M. V. Smoluchowski, Ann. Phys. (Leipzig) **64**, 101 (1898); (b) H. Grad, Comm. Pure Appl. Math. **2**, 331 (1949); (c) P. Welander, Ark. Fys. **7**, 507 (1954); (d) E. P. Gross, E. A. Jackson, and S. Ziering, Ann. Phys. (N.Y.) **1**, 141 (1957); (e) J. R. Dorfman and H. van Beijren, in *Statistical Mechanics,* edited by B. J. Berne (Plenum, New York, 1977), Part B, pp. 65–179.
[21]See, for example, F. O. Goodman and H. Y. Wachman, *Dynamics of Gas Surface Scattering* (Academic, New York, 1976).
[22]See, for example, Chem. Rev. **87** (1987), where a number of experimental and theoretical aspects are extensively reviewed. For theory see R. B. Gerber, Chem. Rev. **87**, 29 (1987).
[23]B. C. Eu, Phys. Rev. A **36**, 400 (1987).
[24]R. E. Khayat and B. C. Eu (unpublished).
[25]G. A. Bird, *Molecular Gas Dynamics* (Oxford, London, 1976).
[26]J. O. Hirschfelder, C. F. Curtiss, and R. B. Bird, *Molecular Theory of Gases and Liquids* (Wiley, New York, 1954).

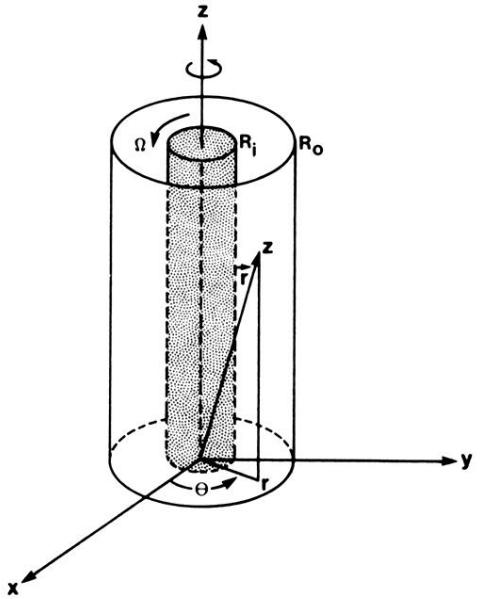

FIG. 1. Coordinates in the cylindrical Couette flow geometry.